



Remote Sensing Analysis of Geologic Hazards

Daniele Giordan ¹, Guido Luzi ², Oriol Monserrat ² and Niccolò Dematteis ^{1,*}¹ Research Institute for Geo-Hydrological Protection, Italian National Research Council, 10135 Turin, Italy² Geomatics Research Unit, Centre Tecnològic de Telecomunicacions de Catalunya, 08860 Castelldefels, Spain

* Correspondence: niccolo.dematteis@irpi.cnr.it

1. Introduction

In recent decades, classical survey techniques (i.e., field measurements and aerial remote sensing) have evolved, and with the advent of new technologies—e.g., terrestrial radar interferometry [1,2], digital time-lapse cameras [3], terrestrial and aerial laser scanners [4,5] and platforms, e.g., UAV [6,7]—remote sensing systems have become popular and widely used in geosciences. Contactless devices are not invasive and allow measuring without accessing the investigated area. This is an excellent advantage as earth surface processes often occur in remote areas and can be potentially dangerous or difficult to access [8]. Satellite and aerial remote sensing offer the possibility of surveying large areas, using hyperspectral optical [8,9], synthetic aperture radar (SAR) [10,11] and thermal infrared [12,13] images and altimetric lasers [14]. The progressive rise in available public and private satellite constellations has permitted individuals to reach very high-resolution images at weekly to daily revisit time. On the other hand, ground-based surveys usually have higher acquisition frequency and spatial resolution compared to satellite systems, and they are able to observe the evolution of fast processes and their possible paroxysmal phase, e.g., volcanic eruptions [15,16], glacier instabilities [17], landslides [18,19], and floods [20,21]. For their characteristics, proximal sensing applications are often used in monitoring activities at a short revisit time, as they can provide real-time or near-real-time information [22]. Therefore, they can be of great support in early warning procedures and risk assessment and management [23,24]. Combined with aerospace sensors, contactless terrestrial devices are particularly suitable for data-fusion techniques, multi-scale approaches and supporting numerical model analysis [25–28].

Satellite and terrestrial remote sensing are of paramount importance in specific tasks of geologic hazard analysis. This Special Issue has collected ten papers concerned with recent and upcoming advances in remote sensing applications in geologic hazard analysis. In particular, this Special Issue includes studies about satellite and terrestrial contactless devices for detecting, monitoring and analyzing geologic processes, as well as new data-processing and warning techniques (Figure 1).



Citation: Giordan, D.; Luzi, G.; Monserrat, O.; Dematteis, N. Remote Sensing Analysis of Geologic Hazards. *Remote Sens.* **2022**, *14*, 4818. <https://doi.org/10.3390/rs14194818>

Received: 16 September 2022

Accepted: 22 September 2022

Published: 27 September 2022

Publisher's Note: MDPI stays neutral with regard to jurisdictional claims in published maps and institutional affiliations.



Copyright: © 2022 by the authors. Licensee MDPI, Basel, Switzerland. This article is an open access article distributed under the terms and conditions of the Creative Commons Attribution (CC BY) license (<https://creativecommons.org/licenses/by/4.0/>).



Figure 1. Word cloud of the abstracts of the contributions of this Special Issue.

2. Contributions of the Special Issue

Satellite and terrestrial remote sensing allow for the analysis of different geological processes and are of paramount importance in specific tasks of hazard analysis. In particular, this Special Issue collects contributions that are concerned with (i) detecting and mapping potential hazards, (ii) acquiring data for analysis of susceptibility and triggering factors, (iii) monitoring the evolution of the process, and (iv) developing strategies of warning and early warning. The considered geological processes are landslides, mining-induced subsidence and land deformations, volcanoes, glacier flows and dune migration. The adopted techniques are varied and include, but are not limited to, optical sensors, SAR, GNSS and multi-sensor approaches (Figure 2). Usually, multi-sensor-based studies use satellite optical images to detect the areas of interest and multitemporal SAR interferometry (MTInSAR) to measure ground deformation in such areas.

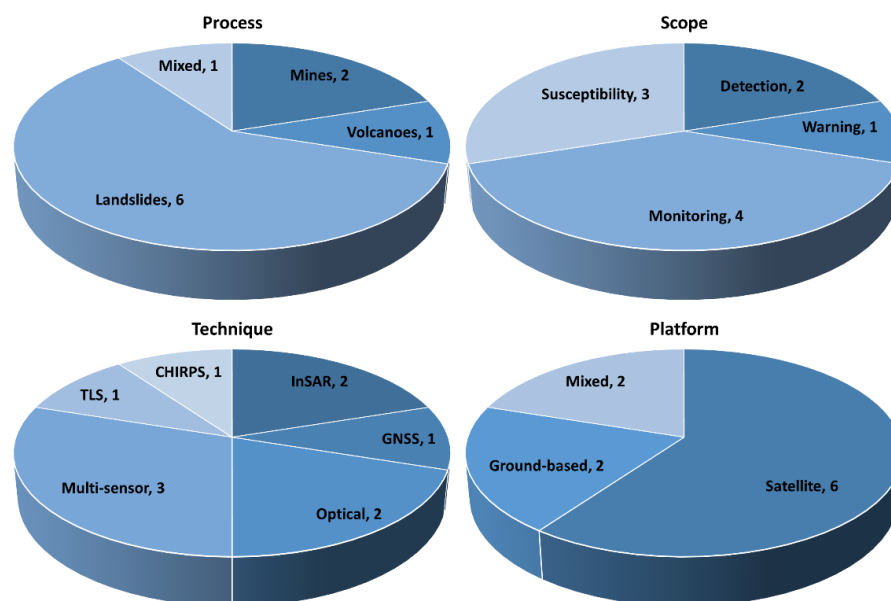


Figure 2. Distributions of the topics dealt with in this Special Issues, according to different schemes of classification: (i) the investigated process, (ii) the scope of the study, (iii) the adopted technique (TLS is terrestrial laser scanner, while CHIRPS is the Climate Hazards group Infrared Precipitation with Stations dataset) and (iv) the platform adopted.

In the following, we will describe the contributions present in this Special Issue. They are organized according to: first, the investigated geologic process, and second, the scope of the study (i.e., detection, monitoring, process analysis and warning).

3. Landslides

Landslides are the most-frequently investigated process in this Special Issue. Six papers examine this phenomenon. However, the studies focus on different themes; some are dedicated to landslide detection [29] and others to triggering factors and susceptibility analysis [30–32], monitoring [33] and early warning procedures [34].

3.1. Detection and Mapping

Lindsay et al. [29] focused their work on landslide mapping. They used optical (Sentinel-2) and SAR (Sentinel-1) satellite images from Google Earth Engine to map the landslides triggered by a rainstorm in western Norway. To detect the landslides, they manually analyzed the differential Normalized Difference Vegetation Index and the SAR amplitude difference of VV and VH polarizations (from the Sentinel-2 and Sentinel-1, respectively). Their results showed that, by using a stack of pre-event images to improve the signal-to-noise ratio, the number of detected landslides increased from 14 (registered by the Norwegian Landslides Inventory) to 120. Moreover, they found that optical images performed better than SAR amplitude images with the aim of landslide detection.

3.2. Process Analysis and Susceptibility

Three works are dedicated to the analysis of triggering factors and susceptibility to landslides and rock slopes. The surveys were conducted from ground, satellite or combined approaches.

Lin et al. [30] studied the spatiotemporal evolution pattern and driving mechanisms of landslides in the Bailong River Basin (China), where a strong earthquake occurred in 2008. They analyzed the period 2007–2020, mapping the occurred landslides using optical images from various sources and measuring the landslide deformation using MTInSAR. They identified three stages of landslide triggering: the earthquake (2008), the coupled earthquake–rainfall (2008–2017), and the rainfall (2017–present) driving stages. In particular, they observed that the landslides in the limestone area were more responsive to the earthquake, while the loess–phyllite-dominated sectors were mainly controlled by rainfall.

The study of Cullen et al. [31] was located in Colombia between 2016 and 2019. They used an inventory of 346 rainfall-induced landslide events and the Climate Hazards group Infrared Precipitation with Stations (CHIRPS) dataset, which combines satellite-based rainfall data and ground-based gauge measurements to produce global rainfall data at a $0.05^\circ \times 0.05^\circ$ resolution. They formulated new dynamic variables based on the rainfall occurrence and amount during dry and wet periods, and determined an original landslide triggering factor (LTF). Comparing their LTF with canonical event–duration threshold, they found that LTF performed better in 81% of cases.

Farmakis et al. [32] analyzed point clouds (PCs) of rock slopes acquired by a terrestrial laser scanner (TLS) in British Columbia (Canada). They partitioned the PCs into voxels based on local dimensionality, orientation, and topology and built an automatic decision tree that utilized geometrical, topological, and contextual information and enabled the classification of a multi-hazard railway rock slope into classes involved in landslide risk management. Their results demonstrated precision similar to more complex machine learning algorithms and manual knowledge-based analysis.

3.3. Monitoring Activities

Bovenga et al. [33] applied MTInSAR to Sentinel-1 and COSMO-SkyMed to measure the velocity time series of two landslides that occurred in 2013 and 2019 in southern Italy, which caused damages to buildings and roads. Their results evidenced the presence of non-linear displacements in correspondence of some key infrastructures. They concluded that

the analysis of accelerations and decelerations of persistent scatter objects corresponding to structures affected by recent stabilization measures helps to shed new light in relation to known events that occurred in the area of interest.

3.4. Warning Procedures

Wu et al. [34] developed a threshold-based early warning procedure for the Gapa Landslide (Southwest China), which was reactivated by the impoundment of a large water reservoir. They observed that the landslide deformation was strongly related to the fluctuations in reservoir water levels; thus, a crucial water level was also defined to reduce false warnings from the velocity threshold alone. The current monitoring system is composed of six permanent GNSS receivers and one water level station. A warning procedure can be activated in case of a velocity exceeding 4 mm day^{-1} and a water level higher than 1820 a.s.l. (i.e., reservoir depth $> 70 \text{ m}$).

4. Mines

Zhang et al. [35] treated the measurement of ground deformation caused by mining activities in the Fengfeng area (Eastern China) in 2015 and 2016. They adopted MTInSAR applied to multiple satellite SAR images, i.e., TerraSAR-X, Sentinel-1, Radarsat-2, and PALSAR-2, thus increasing the data adopted to build the time series. They focused their study on vegetated areas, where MTInSAR observations are usually critical. They measured subsidence of almost 800 mm year^{-1} , and registered a root mean squared deviation of 83 mm year^{-1} compared to terrestrial observations.

Solari et al. [36] applied MTInSAR in a mining area in southern Italy to measure the deformation time series caused by subsidence in the period 2016–2018. They found areas with deformation rates up to 250 mm year^{-1} . Moreover, they manually mapped more than 100 sinkholes that occurred in the area between 1956 and 2018 using nine orthoimages acquired across this period, and they analyzed the deformation in correspondence of the sinkholes. In their work, quite homogeneous subsidence rates ($10\text{--}20 \text{ mm year}^{-1}$) were measured, except for the more recent sinkholes, where the velocities were more heterogeneous and higher (up to 80 mm year^{-1}).

5. Volcanoes

The work of Rosch and Plank [37] concerned the mapping of lava and ash deposits using PlanetScope optical images. This study introduced an object-oriented classification for mapping lava flows in vegetated and unvegetated areas during several eruptive phases of three Indonesian volcanoes. A change detection investigation was combined with the analysis of variations in texture and brightness, with hydrological runoff modelling and with analysis of thermal anomalies derived from Sentinel-2 or Landsat-8. The results showed good agreement with the reports of the Global Volcanism Program and showed the benefits of PlanetScope images for volcano daily monitoring and eruption risk assessment.

6. Glaciers and Sand Dunes

Dematteis and Giordan [38] conducted a methodological study that compared the performances of fifteen digital image correlation functions and proposed a new similarity index (DOT). They analyzed the outcomes considering four template sizes and thirteen types and levels of noise applied on a shaded relief of a digital elevation. They conducted the same comparison on optical images of a glacier (acquired by a terrestrial camera) and the dunes of the Bodélé Depression (Chad) (acquired by Sentinel-2). Overall, they observed that using orientation images provided the best performances in the presence of shadows or snow patches, adopting either frequency-based or DOT correlations.

7. Conclusions

This Special Issue consists of ten papers that used remote sensing (either from ground or aerospace) to analyze geologic hazards. The applied techniques are varied and include

GNSS, TLS, SAR, optical images and rainfall datasets. On several occasions, multi-sensor approaches were adopted. The scopes are different as well, and they can be summarized in four classes: (i) detection, (ii) susceptibility and triggering factors analysis, (iii) monitoring, and (iv) early warning. Considering all the contributions, this Special Issue demonstrates the high benefit of using remote sensing to analyze geologic hazards and represents a valuable advance of the research in this field.

Author Contributions: Writing—original draft preparation, N.D.; writing—review and editing, D.G., G.L., O.M. and N.D. All authors have read and agreed to the published version of the manuscript.

Funding: This research received no external funding.

Acknowledgments: The Guest Editors of this Special Issue would like to thank all authors who have contributed to this volume for sharing their scientific results and for their excellent collaboration. Special gratitude will go to the community of distinguished reviewers for their constructive inputs. The Remote Sensing editorial team is acknowledged for its support during all phases related to the successful completion of this issue.

Conflicts of Interest: The authors declare no conflict of interest.

References

1. Monserrat, O.; Crosetto, M.; Luzi, G. A review of ground-based SAR interferometry for deformation measurement. *ISPRS J. Photogramm. Remote Sens.* **2014**, *93*, 40–48. [[CrossRef](#)]
2. Caduff, R.; Schlunegger, F.; Kos, A.; Wiesmann, A. A review of terrestrial radar interferometry for measuring surface change in the geosciences. *Earth Surf. Process. Landf.* **2015**, *40*, 208–228. [[CrossRef](#)]
3. Travelletti, J.; Delacourt, C.; Allemand, P.; Malet, J.P.; Schmittbuhl, J.; Toussaint, R.; Bastard, M. Correlation of multi-temporal ground-based optical images for landslide monitoring: Application, potential and limitations. *ISPRS J. Photogramm. Remote Sens.* **2012**, *70*, 39–55. [[CrossRef](#)]
4. Baldo, M.; Bicocchi, C.; Chiocchini, U.; Giordan, D.; Lollino, G. LIDAR monitoring of mass wasting processes: The Radicofani landslide, Province of Siena, Central Italy. *Geomorphology* **2009**, *105*, 193–201. [[CrossRef](#)]
5. Giordan, D.; Allasia, P.; Manconi, A.; Baldo, M.; Santangelo, M.; Cardinali, M.; Corazza, A.; Albanese, V.; Lollino, G.; Guzzetti, F. Morphological and kinematic evolution of a large earthflow: The Montaguto landslide, southern Italy. *Geomorphology* **2013**, *187*, 61–79. [[CrossRef](#)]
6. Colomina, I.; Molina, P. Unmanned aerial systems for photogrammetry and remote sensing: A review. *ISPRS J. Photogramm. Remote Sens.* **2014**, *92*, 79–97. [[CrossRef](#)]
7. Giordan, D.; Adams, M.S.; Aicardi, I.; Alicandro, M.; Allasia, P.; Baldo, M.; De Berardinis, P.; Dominici, D.; Godone, D.; Hobbs, P.; et al. The use of unmanned aerial vehicles (UAVs) for engineering geology applications. *Bull. Eng. Geol. Environ.* **2020**, *79*, 3437–3481. [[CrossRef](#)]
8. Leprince, S.; Berthier, E.; Ayoub, F.; Delacourt, C.; Avouac, J.P. Monitoring earth surface dynamics with optical imagery. *Eos* **2008**, *89*, 1–2. [[CrossRef](#)]
9. Van der Meer, F.; Freek, D. Multi-and hyperspectral geologic remote sensing: A review. *Int. J. Appl. Earth Obs. Geoinf.* **2012**, *14*, 112–128. [[CrossRef](#)]
10. Cigna, F.; Osmanoğlu, B.; Cabral-Cano, E.; Dixon, T.H.; Ávila-Olivera, J.A.; Garduño-Monroy, V.H.; DeMets, C.; Wdowinski, S. Monitoring land subsidence and its induced geological hazard with Synthetic Aperture Radar Interferometry: A case study in Morelia, Mexico. *Remote Sens. Environ.* **2012**, *117*, 146–161. [[CrossRef](#)]
11. Shen, X.; Wang, D.; Mao, K.; Anagnostou, E.; Hong, Y. Inundation extent mapping by synthetic aperture radar: A review. *Remote Sens.* **2019**, *11*, 879. [[CrossRef](#)]
12. Gerhards, M.; Schlerf, M.; Mallick, K.; Udelhoven, T. Challenges and future perspectives of multi-/Hyperspectral thermal infrared remote sensing for crop water-stress detection: A review. *Remote Sens.* **2019**, *11*, 1240. [[CrossRef](#)]
13. Weng, Q. Thermal infrared remote sensing for urban climate and environmental studies: Methods, applications, and trends. *ISPRS J. Photogramm. Remote Sens.* **2009**, *64*, 335–344. [[CrossRef](#)]
14. Neumann, T.A.; Martino, A.J.; Markus, T.; Bae, S.; Bock, M.R.; Brenner, A.C.; Brunt, K.M.; Cavanaugh, J.; Fernandes, S.T.; Hancock, D.W.; et al. The Ice, Cloud, and Land Elevation Satellite—2 mission: A global geolocated photon product derived from the advanced topographic laser altimeter system. *Remote Sens. Environ.* **2019**, *233*, 111325. [[CrossRef](#)]
15. Casagli, N.; Tibaldi, A.; Merri, A.; Del Ventisette, C.; Apuani, T.; Guerri, L.; Fortuny-Guasch, J.; Tarchi, D. Deformation of Stromboli Volcano (Italy) during the 2007 eruption revealed by radar interferometry, numerical modelling and structural geological field data. *J. Volcanol. Geotherm. Res.* **2009**, *182*, 182–200. [[CrossRef](#)]
16. Honda, K.; Nagai, M. Real-time volcano activity mapping using ground-based digital imagery. *ISPRS J. Photogramm. Remote Sens.* **2002**, *57*, 159–168. [[CrossRef](#)]

17. Dematteis, N.; Giordan, D.; Troilo, F.; Wrzesniak, A.; Godone, D. Ten-Year Monitoring of the Grandes Jorasses Glaciers Kinematics. Limits, Potentialities, and Possible Applications of Different Monitoring Systems. *Remote Sens.* **2021**, *13*, 3005. [[CrossRef](#)]
18. Uhlemann, S.; Smith, A.; Chambers, J.; Dixon, N.; Dijkstra, T.; Haslam, E.; Meldrum, P.; Merritt, A.; Gunn, D.; Mackay, J. Assessment of ground-based monitoring techniques applied to landslide investigations. *Geomorphology* **2016**, *253*, 438–451. [[CrossRef](#)]
19. Pecoraro, G.; Calvello, M.; Piciullo, L. Monitoring strategies for local landslide early warning systems. *Landslides* **2019**, *16*, 213–231. [[CrossRef](#)]
20. Lo, S.W.; Wu, J.H.; Lin, F.P.; Hsu, C.H. Visual sensing for urban flood monitoring. *Sensors* **2015**, *15*, 20006–20029. [[CrossRef](#)]
21. Perks, M.T.; Russell, A.J.; Large, A.R.G. Technical note: Advances in flash flood monitoring using unmanned aerial vehicles (UAVs). *Hydrol. Earth Syst. Sci.* **2016**, *20*, 4005–4015. [[CrossRef](#)]
22. Casagli, N.; Catani, F.; Del Ventisette, C.; Luzi, G. Monitoring, prediction, and early warning using ground-based radar interferometry. *Landslides* **2010**, *7*, 291–301. [[CrossRef](#)]
23. Intrieri, E.; Gigli, G.; Mugnai, F.; Fanti, R.; Casagli, N. Design and implementation of a landslide early warning system. *Eng. Geol.* **2012**, *147–148*, 124–136. [[CrossRef](#)]
24. Manconi, A.; Giordan, D. Landslide early warning based on failure forecast models: The example of the Mt. de la Saxe rockslide, northern Italy. *Nat. Hazards Earth Syst. Sci.* **2015**, *15*, 1639–1644. [[CrossRef](#)]
25. Malet, J.P.; Ferhat, G.; Ulrich, P.; Boetzelé, P. The French National Landslide Observatory OMIV—Monitoring surface displacement using permanent GNSS, photogrammetric cameras and terrestrial LiDAR for understanding the landslide mechanisms. In Proceedings of the 3rd Joint International Symposium on Deformation Monitoring (JISDM), Vienne, Austria, 7 May 2016; pp. 1–7.
26. Casagli, N.; Frodella, W.; Morelli, S.; Tofani, V.; Ciampalini, A.; Intrieri, E.; Raspini, F.; Rossi, G.; Tanteri, L.; Lu, P. Spaceborne, UAV and ground-based remote sensing techniques for landslide mapping, monitoring and early warning. *GeoenvIRON. Disasters* **2017**, *4*, 9. [[CrossRef](#)]
27. Lollino, P.; Giordan, D.; Allasia, P. The Montaguto earthflow: A back-analysis of the process of landslide propagation. *Eng. Geol.* **2014**, *170*, 66–79. [[CrossRef](#)]
28. Musa, Z.N.; Popescu, I.; Mynett, A. A review of applications of satellite SAR, optical, altimetry and DEM data for surface water modelling, mapping and parameter estimation. *Hydrol. Earth Syst. Sci.* **2015**, *19*, 3755–3769. [[CrossRef](#)]
29. Lindsay, E.; Frauenfelder, R.; Rütger, D.; Nava, L.; Rubensdotter, L.; Strout, J.; Nordal, S. Multi-Temporal Satellite Image Composites in Google Earth Engine for Improved Landslide Visibility: A Case Study of a Glacial Landscape. *Remote Sens.* **2022**, *14*, 2301. [[CrossRef](#)]
30. Lin, L.; Chen, G.; Shi, W.; Jin, J.; Wu, J.; Huang, F.; Chong, Y.; Meng, Y.; Li, Y.; Zhang, Y. Spatiotemporal Evolution Pattern and Driving Mechanisms of Landslides in the Wenchuan Earthquake-Affected Region: A Case Study in the Bailong River Basin, China. *Remote Sens.* **2022**, *14*, 2339. [[CrossRef](#)]
31. Cullen, C.A.; Al Suhili, R.; Aristizabal, E. A Landslide Numerical Factor Derived from CHIRPS for Shallow Rainfall Triggered Landslides in Colombia. *Remote Sens.* **2022**, *14*, 2239. [[CrossRef](#)]
32. Farmakis, I.; Bonneau, D.; Hutchinson, D.J.; Vlachopoulos, N. Targeted rock slope assessment using voxels and object-oriented classification. *Remote Sens.* **2021**, *13*, 1354. [[CrossRef](#)]
33. Bovenga, F.; Argentiero, I.; Refice, A.; Nutricato, R.; Nitti, D.O.; Pasquariello, G.; Spilotro, G. Assessing the Potential of Long, Multi-Temporal SAR Interferometry Time Series for Slope Instability Monitoring: Two Case Studies in Southern Italy. *Remote Sens.* **2022**, *14*, 1677. [[CrossRef](#)]
34. Wu, S.; Hu, X.; Zheng, W.; Berti, M.; Qiao, Z.; Shen, W. Threshold definition for monitoring Gapa Landslide under large variations in reservoir level using GNSS. *Remote Sens.* **2021**, *13*, 4977. [[CrossRef](#)]
35. Zhang, B.; Wu, S.; Ding, X.; Wang, C.; Zhu, J.; Li, Q. Use of multiplatform sar imagery in mining deformation monitoring with dense vegetation coverage: A case study in the fengfeng mining area, china. *Remote Sens.* **2021**, *13*, 3091. [[CrossRef](#)]
36. Solari, L.; Montalti, R.; Barra, A.; Monserrat, O.; Bianchini, S.; Crosetto, M. Multi-temporal satellite interferometry for fast-motion detection: An application to salt solution mining. *Remote Sens.* **2020**, *12*, 3919. [[CrossRef](#)]
37. Rösch, M.; Plank, S. Detailed Mapping of Lava and Ash Deposits at Indonesian Volcanoes by Means of VHR PlanetScope Change Detection. *Remote Sens.* **2022**, *14*, 1168. [[CrossRef](#)]
38. Dematteis, N.; Giordan, D. Comparison of digital image correlation methods and the impact of noise in geoscience applications. *Remote Sens.* **2021**, *13*, 327. [[CrossRef](#)]